Invariant-ability of the PSF of wide-field microscopy to the DOF by using cubic phase mask

Minhnghia Pham[1], Vannhu Le[1,*], Huykien Le[1] and Synam Truong[2]
[1]Le Quy Don Technical University Hanoi, Vietnam
[2]Hatinh Medical College, HaTinh, Vietnam

[*]Corresponding author

***Abstract*—: In this paper, we have suggested the new technique for the improvement of the invariant ability of the point spread function (PSF) of wide-field microscopy to the depth of field (DOF). When a cubic phase mask (CPM) is inserted in the exist-pupil position of the imaging system, the invariant-ability of the point spread function (PSF) to the DOF is enhanced. The comparison for the invariant-ability of the PSFs for the traditional imaging system (IMS) and the CPM to the DOF are presented. Moreover, the experimental setup of the IMS is built. The experimental results are shown and agree with the simulation results.**

Keywords— Wavefront coding, the depth of field, imaging system

I. INTRODUCTION

The IMS specified the number aperture has the given depth-of-field as shown in Fig. 1. Only image of the objects over this DOF is clear and sharp [1-3]. Whereas, the image of the objects inside the DOF is blurred. When we use wide-field microscopy views the sample. The image of the sample outside the DOF becomes the background-noise, which causes the blurring to the captured image [4]. In order to achieve more obvious image, the sample is thin because the background-noise is reduced. However, the background-noise of the focus-outside image is not avoided. We know that wide-field microscopy is usually used to analyze the 3D sample. For the big DOF, we can obtain much truth information of the real object [5]. As well know that the DOF is equal to $2\lambda/NA^2$ and the lateral resolution is set to $0.61\lambda/NA$, where λ is the light wavelength; NA the number aperture [6, 7]. The DOF can be improved by reducing the NA value. This is corresponding to the point spread function slowly changing to the DOF. Nevertheless, the lateral resolution is reduced. This means that the separated-ability of the IMS is reduced.

The IMS with the widely DOF has been used in many practical applications. For infrared imaging systems, the index refraction has sensitive to temperature change. When temperature changes, the focal plane is shifted. This produces the reduction of image quality of imaging system. The IMS with the widely DOF can be applied in infrared imaging systems in order to acquire the imaging ability invariant over a wide range of temperature-change, so the effect of temperature change can be corrected [8-12]. In order to obtain the imaging ability with super-resolution and large DOF, the IMS with the widely range of the DOF is combined with super-resolution techniques as shown in Refs. [13-15]. For light sheet fluorescence microscopy, there are trade-off between both the thickness and the field of view.

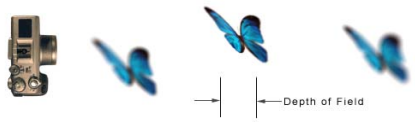

Fig. 1 The given images at the different positions for the DOF in the IMS.

The wide range of the DOF is used to enhance the field of view in 3D imaging of light sheet fluorescence microscopy [16-18]. The IMS with the wide range of the DOF is used for correcting aberrations including Petzval curvature, astigmatism, assembly related missfocus, spherical and chromatic aberration [19-22]. Other application of The IMS with the wide range of the DOF is in zoom IMS [23, 24]. In zoom IMS with the big range of the DOF, only an optical component requires shift, so the IMS is simple and perform easy. However, the image quality is also ensured.

Here, we introduce a novel technique for the enhancement of the DOF of the imaging system, which was called wavefront coding technique (WFC). In WFC technique, a phase mask is added the exist pupil position of the imaging system. When the phase mask which is inserted in the IMS has the kind of the CPM, the invariant-ability of the PSF or the optical transfer function (OTF) over a widely range of the DOF is enhanced. However, the size of the PSF spreads in comparison to that of diffraction limited PSF. We can employ the WFC technique to achieve the improvement of the DOF about 7 times in comparison with the traditional imaging system.

II. THEORY

The phase pupil function of the IMS combining the CPM and defocus parameter is represented by:

$$P(x,y)=\begin{cases}\dfrac{1}{\sqrt{2}}\exp[i(ax^3+ay^3+\psi x^2+\psi y^2)] & \text{if } x^2+y^2\le 1\\ 0 & \text{other}\end{cases} \quad (1)$$

Where both x and y are the normalized coordinates at the pupil plane position, the CPM can be presented by:

XXX-X-XXXX-XXXX-X/XX/$XX.00 ©20XX IEEE
978-1-7281-6866-1/20/$31.00 ©2020 IEEE

$$f(x,y)=\begin{cases} ax^3+ay^3 & \text{if } x^2+y^2\le 1 \\ 0 & \text{other} \end{cases} \quad (2)$$

and ψ is the defocus parameter and can be presented by

$$\psi=\frac{\pi L^2}{4\lambda}\left(\frac{1}{f}-\frac{1}{d_0}-\frac{1}{d_i}\right)=\frac{2\pi}{\lambda}W_{20}=kW_{20} \quad (3)$$

where $k = 2\pi/\lambda$; λ denotes the light wavelength; W_{20} is measured in unit of light wavelength; L denotes the length of the lens aperture; the distance d_0 denotes the distance from the first principal plane of the lens to the object; the distance d_i denotes the distance from the second principal plane to the image plane. By varying the amount of d_0, the amount of the DOF, Δ, is generated.

The PSF, h, of the IMS to defocus parameter can be expressed by:

$$h(x_0,y_0,\psi)=\left|FFT[P(x,y,\psi)]\right|^2 \quad (4)$$

where x_0 and y_0 are the normalized coordination at the imaging plane.

The intensity image, g, captured by one detector can be expressed as:

$$g=o*h+n \quad (5)$$

where o is the object and n is the noise; $*$ is convolution operator.

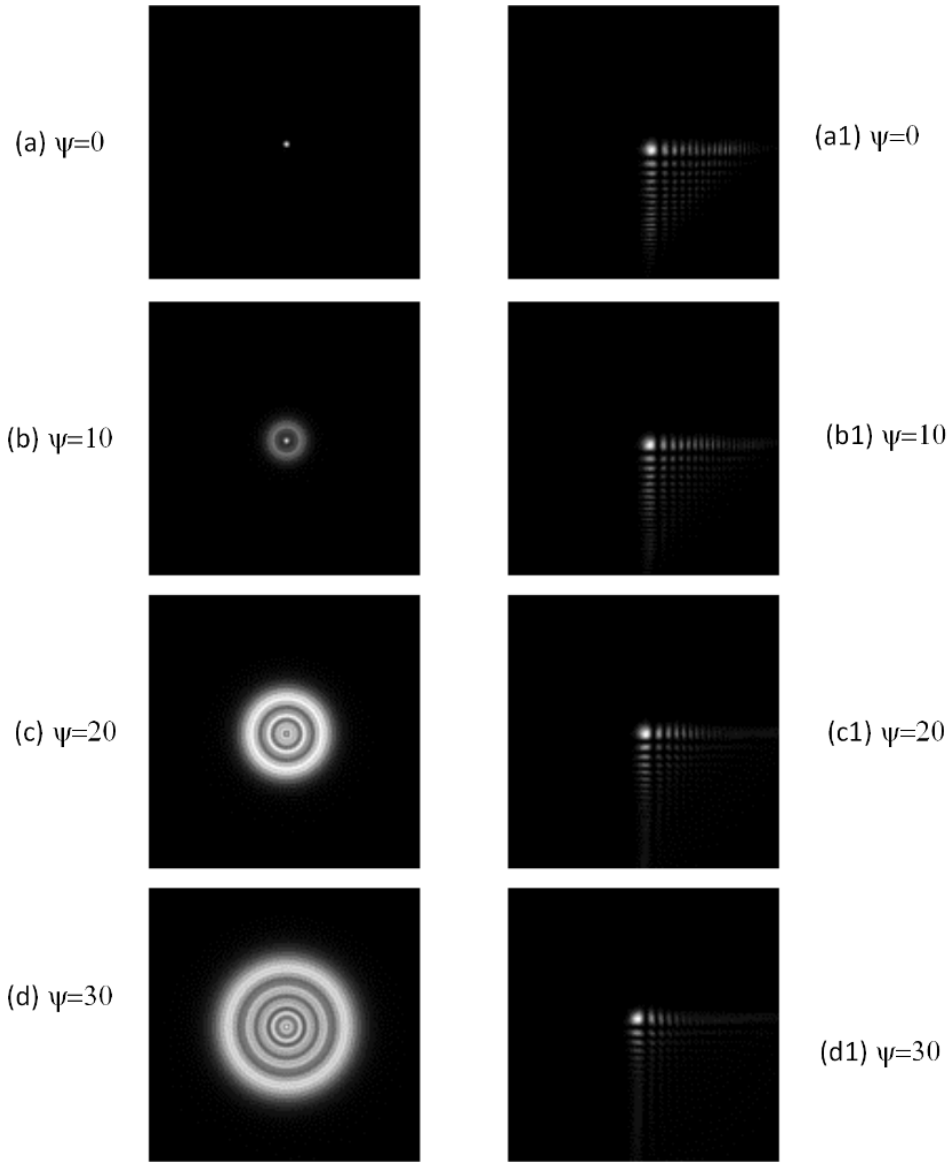

Fig. 2 The change of the PSFs of both the traditional IMS and the CPM to defocus parameter. The left images for the traditional IMS and the right images for the CPM.

As shown Eq. (5), the image-quality depends on the PSF. In order to show the deferent change of both the PSF of the CPM and the PSF of the traditional IMS to defocus parameter, inhere, we show some simulation results with the PSFs. By using the Eq. (4), the change of both the PSFs of the CPM with a=30 and the traditional IMS to defocus

parameter are indicated in Fig. 2, where ψ value is set to 0, 10, 20 and 30. It is not difficult to see that the sizes of the PSFs of the traditional IMS varies quickly for the change of defocus parameter. When the defocus parameter is set to ψ=0, the size of the PSF of the traditional IMS is the smallest as depicted in Fig. 2(a). However, the defocus parameter is increasing, the sizes of the PSFs of the traditional IMS fast change as shown in Figs. 2(b)-2(d). It is clear that the PSFs of the CPM keep the size and shape invariant to defocus. However, the sizes of the PSF of the CPM is very bigger than that of the PSF of the traditional IMS at the defocus parameter of ψ=0.

III. EXPERIMENTAL RESULTS

The experimental layout of the IMS is indicated in Fig. 3. Laser source laser He-Ne with λ = 632,8 nm (1) generates a parable beam. The filter (2) control the intensity of the parable beam. This beam is focused by the objective lens (3) with *NA*=0.56. A pinhole with size of 25µm (4) is placed at the focus positon of the objective lens, 3. A lens with focus length of f'= 150 mm (5) generates a parable beam in behind of this lens. An aperture (6) controls the size of the beam. After the aperture (6), we place an objective lens (7) with *NA* =0,65 to crease a light dot which is corresponding to the point object in the focus plane. The objective lens (8) with *NA*=0.25, $10^{\times}$, will build the point object on the detector (10). After the object (8), the CPM with *a*=30 is placed after the objective lens (8). The size of detector is set to 6177µm ×4650 µm. The detector is connected with computer. The objective lens (8), phase mask (9) and detector (10) are placed on the shift set (11) with set of 1µm.

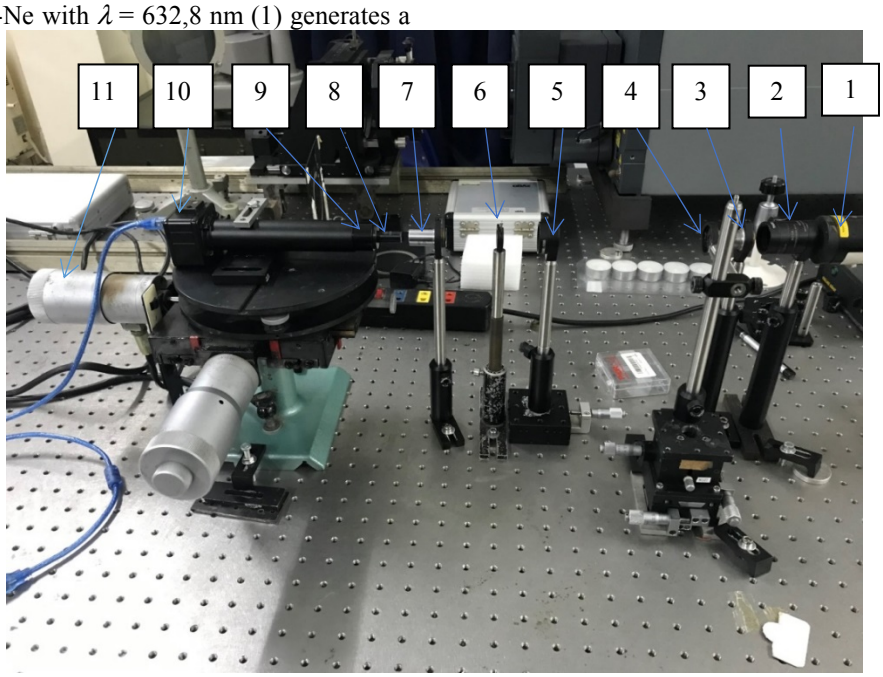

Fig 3. The experimental setup of the IMS to measure the PSF.

In order to measure the PSF at the difference positions of the depth-of-field, we control the shift set. When we measure the PSF for the traditional imaging system, the CPM is not presented the experimental system. The measured results of The PSF are shown in Fig. 4. It can be seen that size of the PSF varies fast when the DOF is increasing. The size of the PSF at the DOF of Δ=0µm is the smallest. These agree with the above simulation results. The DOF of the objective lens of NA=0.25 is nearly set to 20µm.

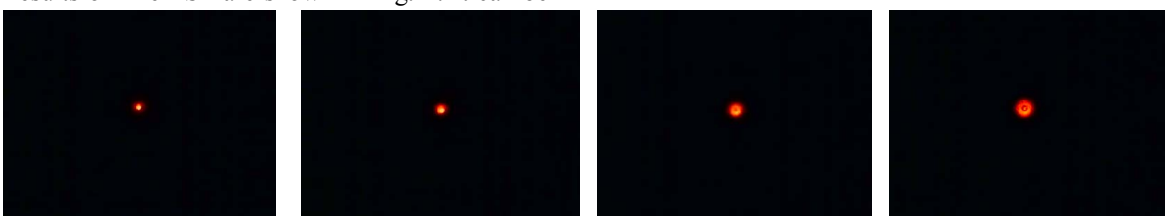

Δ=0 (a) Δ=10µm (b) Δ=20µm(c) Δ=30µm (d)

Fig. 4. The PSFs of the traditional IMS at difference positions of the DOF.

For the CPM, the measured results of the PSF at the difference positions of the DOF are depicted in Fig. 5. It is not difficult to see that the PSFs are nearly invariant to vary the widely range of the DOF form 0µm to 70µm, so the CPM can be used to be set to the widely range of the DOF about 140µm. This means that the CPM can be employed to achieve the improvement of the DOF about 7 times in comparison to the traditional imaging system. However, the size of the PSF of the CPM spreads in comparison of that of the PSF of the traditional IMS at the DOF of Δ=0µm. These

results agree with the above simulation results. However, there is one difference between both the simulation result and the experimental results, this is the rotating of the PSF. The rotating generates by rotating of the CPM around z axis in the experimental model comparison to the theory model.

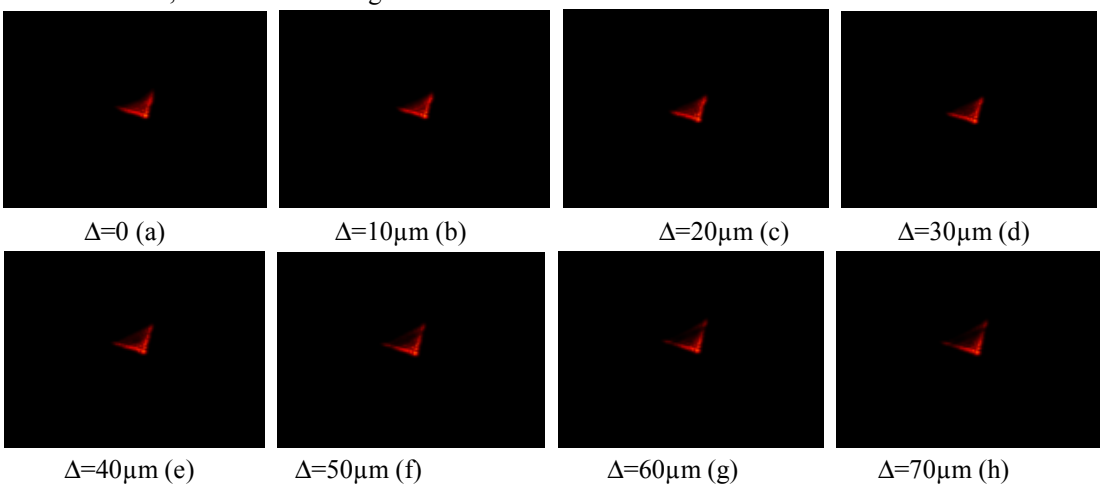

Fig. 5. The PSFs of the CPM at difference positions of the DOF.

Another way is used to show the ability invariant for the change the depth of filed to be the evaluation of the change of the peak intensity along z axis. The peak intensity of the traditional IMS is measured by the intensity of the PSF on the z axis. The peak intensity of the PSFs of the CPM is measured by the peak intensity of the first dot of the PSFs of the CPM. The maximum intensity peaks of the PSFs of the traditional IMS and the CPM is normalized by one. The intensity distribution along z axis is shown in Fig. 6. The intensity distribution of the traditional IMS along z axis reduces quickly the change of the DOF. While, the intensity distribution of the CPM is invariant over a wide range of DOF.

The finally, the 3D PSF of the traditional IMS and the CPM is indicated. The 3D PSFs of the traditional IMS and the CPM are indicated in Fig. 7. The PSF of the traditional IMS changes quickly to the DOF. Whereas, the PSF of the CPM is the invariance over the widely range of the DOF. The peak intensity of the PSF of the CPM shifts on a bending line along z optical axis.

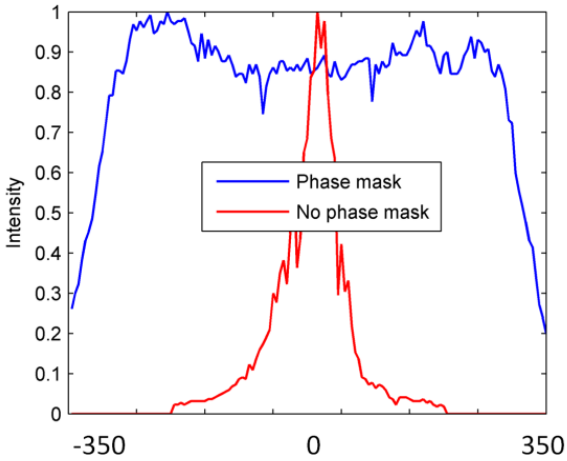

Fig. 6. The intensity distribution of the traditional IMS and the CPM along the z axis.

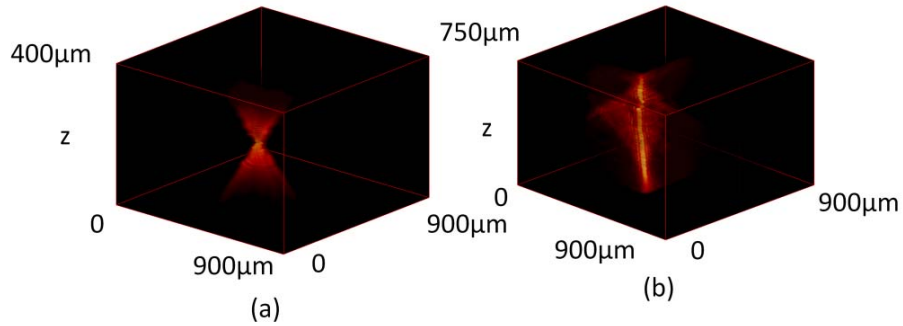

Fig. 7 the 3D PSF of the traditional IMS and the CPM.

IV. CONCLUSION

In summary, we have introduced a powerful technique to obtain the improvement of invariant ability of the PSF over a big range of depth of filed, in which the CPM has been added in the imaging system. The experimental layout of the IMS is built to measure the PSF. The measured results of the PSFs are presented. The experimental results proved that the CPM can be used to acquire the enhancement of the DOF about 7 times in comparison with the traditional imaging system. In future, some practical applications will be acquired.

ACKNOWLEDGMENT

This work is supported by Vietnam National Foundation for Science and Technology Development (NAFOSTED) under Grant number (103.03-2018.08).

REFERENCES

[1] R. Hild, M J. Yzuel, J C. Escalera, et al., "Influence of Nonuniform Pupils in Imaging Periodical Structures by Photolithographic Systems," Optical Engineering, 37(4), pp. 1353-1363, 1998.

[2] J. Campos, J C. Escalera, R. Hild, et al., "The Asseesment of Nnuniform Pupils in Photolithography," Microelectronic Engineering, 30(14), pp. 103 – 106, 1996.

[3] R. Hild, M J. Yzuel, J C. Escalera, "High Focal Depth Imaging of Small Structures," Microelectronic Engineering, 34(2), pp. 195-214, 1997.

[4] R. Narayanswamy, G E. Johnson, P E X. Silveira, et al., "Extending the Imaging Volume for Biometric Iris Recognition," Applied Optics, 44(5), pp. 701-712, 2005.

[5] Hart, C. Douglas, "*The Camera Assistant: A Complete Professional Handbook*," Newton, MA: Focal Press, 1996, ISBN 0-240-80042-7.

[6] https://www.edmundoptics.com/knowledge-center/application-notes/imaging/depth-of-field-and-depth-of-focus/

[7] https://www.slrlounge.com/aperture-guide-pt2-shallow-and-deep-depth-of-field/

[8] K. Kubala, E. Dowski, W. Cathey, "Reducing complexity in computational imaging systems," Optics Express, Vol. 11, Issue 18, pp. 2102-2108, 2003.

[9] S. Chen, Z. Fan, Z. Xu, et al., "Wavefront coding technique for controlling thermal defocus aberration in an infrared imaging system," Optics Letters, Vol. 36, Issue 16, 2011, pp. 3021-3023.

[10] S. Bradburn, W. T. Cathey, E. R. Dowski, "Realizations of focus invariance in optical-digital systems with wave-front coding," Applied Optics, Vol. 36, Issue 35, pp. 9157-9166, 1997.

[11] B. Feng, Z. Shi, B. Xu, et al., "ZnSe-material phase mask applied to athermalization of infrared imaging systems," Applied Optics, Vol. 55, Issue 21, pp. 5715-5720, 2016.

[12] B. Feng, Z. Shi, Y. Zhao, et al., "A wide-FoV athermalized infrared IMS with a two-element lens," Infrared Physics & Technology, Vol. 87, pp. 11-21, 2017.

[13] Y. Zhou, P. Zammit, G. Carles, et al., "Computational localization microscopy with extended axial range," Optics Express, Vol. 26, Issue 6, pp. 7563-7577, 2018.

[14] S. Jia, J. C. Vaughan, X. Zhuang, "Isotropic three-dimensional super-resolution imaging with a self-bending point spread function," Nature Photonics, Vol. 8, pp. 302-306, 2014.

[15] B. Schroeder, S. Jia, "Frequency analysis of a self-bending point spread function for 3D localization-based optical microscopy," Optics Letters, Vol. 40, Issue 13, pp. 3189-3192, 2015.

[16] T. Vettenburg, H. I. C. Dalgarno, J. Nylk, et al., "Light-sheet microscopy using an Airy beam," Nature Method, Vol. 11, pp. 541-544, 2014.

[17] S. Quirin, N. Vladimirov, C. T. Yang, et al., "Calcium imaging of neural circuits with extended depth-of-field light-sheet microscopy, *Optica*, Vol. 41, Issue 5, pp. 855-858, 2016.

[18] O. E. Olarte, J. Andilla, D. Artigas, et al., Decoupled illumination detection in light sheet microscopy for fast volumetric imaging," Optica, Vol. 2, Issue 8, pp. 702-705, 2015.

[19] H. B. Wach, E. R. Dowski, W. T. Cathey, "Control of chromatic focal shift through wave-front coding," Applied Optics, Vol. 37, Issue 23, pp. 5359-5367, 1998.

[20] E. Dowski, K. Kubala, "Reducing size, weight, and cost in a LWIR IMS with wavefront coding," Proceedings of SPIE, Vol. 5407, pp. 66-73, 2004.

[21] G. Saavedra, I. Escobar, R. Martinez-Cuenca, et al., "Reduction of spherical-aberration impact in microscopy by wavefront coding," Optics Express, Vol. 17, Issue 16, pp. 13810-13818, 2009.

[22] J. Arines, R. O. Hernandez, S. Sinzinger, "Wavefront-coding technique for inexpensive and robust retinal imaging," Optics Letters, Vol. 39, Issue 13, pp. 3986-3988, 2014.

[23] M. Demenikov, E. Findlay, A. R. Harvay, "Miniaturization of zoom lenses with a single moving element," Optics Express, Vol. 17, Issue 8, pp. 6118-6127, 2009.

[24] M. Demenikov, E. Findlay, A. R. Harvay, "Experimental demonstration of hybrid imaging for miniaturization of an optical zoom lens with a single moving element," Optics Express, Vol. 36, Issue 6, pp. 969-971, 2011.